

# Nuclear Charge Radii of $^{7,9,10}\text{Be}$ and the one-neutron halo nucleus $^{11}\text{Be}$

W. Nörtershäuser,<sup>1,2</sup> D. Tiedemann,<sup>2</sup> M. Žáková,<sup>2</sup> Z. Andjelkovic,<sup>2</sup> K. Blaum,<sup>3</sup> M. L. Bissell,<sup>4</sup> R. Cazan,<sup>2</sup> G.W.F. Drake,<sup>5</sup> Ch. Geppert,<sup>6,7</sup> M. Kowalska,<sup>8</sup> J. Krämer,<sup>2</sup> A. Krieger,<sup>2</sup> R. Neugart,<sup>2</sup> R. Sánchez,<sup>6</sup> F. Schmidt-Kaler,<sup>9</sup> Z.-C. Yan,<sup>10</sup> D. T. Yordanov,<sup>3</sup> and C. Zimmermann<sup>7</sup>

<sup>1</sup>*GSI Helmholtzzentrum für Schwerionenforschung GmbH, D-64291 Darmstadt, Germany*

<sup>2</sup>*Institut für Kernchemie, Universität Mainz, D-55128 Mainz, Germany*

<sup>3</sup>*Max-Planck-Institut für Kernphysik, D-69117 Heidelberg, Germany*

<sup>4</sup>*Instituut voor Kern- en Stralingsfysica, Katholieke Universiteit Leuven, B-3001 Leuven, Belgium*

<sup>5</sup>*Department of Physics, University of Windsor, Windsor, Ontario, Canada, N9B 3P4*

<sup>6</sup>*Helmholtzzentrum für Schwerionenforschung GmbH, D-64291 Darmstadt, Germany*

<sup>7</sup>*Physikalisches Institut, Universität Tübingen, D-72076 Tübingen, Germany*

<sup>8</sup>*CERN, Physics Department, CH-1211 Geneva 23, Switzerland*

<sup>9</sup>*Quanteninformationsverarbeitung, Universität Ulm, D-89069 Ulm, Germany*

<sup>10</sup>*Department of Physics, University of New Brunswick, Fredericton, New Brunswick, Canada E3B 5A3*

(Dated: May 28, 2018)

Nuclear charge radii of  $^{7,9,10,11}\text{Be}$  have been determined by high-precision laser spectroscopy. On-line measurements were performed with collinear laser spectroscopy in the  $2s_{1/2} \rightarrow 2p_{1/2}$  transition on a beam of  $\text{Be}^+$  ions. Collinear and anticollinear laser beams were used simultaneously and the absolute frequency determination using a frequency comb yielded an accuracy in the isotope-shift measurements of about 1 MHz. Combination with accurate calculations of the mass-dependent isotope shifts yield nuclear charge radii. The charge radius decreases from  $^7\text{Be}$  to  $^{10}\text{Be}$  and then increases for the halo nucleus  $^{11}\text{Be}$ . When comparing our results with predictions of *ab initio* nuclear structure calculations we find good agreement. Additionally, the nuclear magnetic moment of  $^7\text{Be}$  was determined to be  $-1.3995(5) \mu_N$  and that of  $^{11}\text{Be}$  from a previous  $\beta$ -NMR measurement was confirmed.

PACS numbers: 32.10.Fn, 21.10.Ft, 27.20.+n, 42.62.Fi, 31.15.ac

The discovery of halo nuclei in 1985 [1] triggered a large number of experiments in order to understand the properties and behavior of these extraordinary systems. In a halo nucleus, individual nucleons - in most cases neutrons - can reside far away from the nuclear core. The best established and investigated neutron-halo nuclei are  $^{6,8}\text{He}$ ,  $^{11}\text{Li}$ , and  $^{11}\text{Be}$ . In a neutron-halo nucleus, the change of the nuclear charge distribution provides information on the interactions between the different subsystems of the strongly clustered nucleus. Such changes may originate from two effects: firstly, the motion of the nuclear core relative to the center of mass, and secondly core polarization induced by the interaction between the halo neutrons and the core. In the case of helium the nuclear core is tightly bound and only a 4% contribution of core excitation is expected [2]. The dominant part of the change is induced by the center-of-mass motion. Conversely, the  $^9\text{Li}$  core in  $^{11}\text{Li}$  is rather soft and core polarization can play a much more important role [3]. Separation between these effects is not trivial since the correlation between the halo neutrons needs to be considered. Thus, to develop a consistent picture of neutron-rich light nuclei, more data are necessary for different systems, which is a motivation to determine accurately the charge radii of  $^{7,9,10,11}\text{Be}$ .  $^{11}\text{Be}$  is the first one-neutron halo nucleus for which the charge radius is reported.

The only known model-independent way to determine charge radii of unstable isotopes is the laser spectroscopic

measurement of the nuclear-volume dependent isotope shift. Nuclear-volume shifts for isotopes of the light elements are very small, and short-lived isotopes can be produced only in marginal quantities. Therefore, high-precision measurements are extremely difficult. Moreover, it is a major challenge to separate these small effects from the mass shifts which dominate by three orders of magnitude. A breakthrough on the theoretical side was the sufficiently accurate calculation of mass shifts for systems with up to three-electrons [4, 5, 6, 7, 8]. These results have been used for the first time to determine the charge radii of  $^{6,7,8,9}\text{Li}$  [9] and  $^6\text{He}$  [10]. Later, the charge radii of the two-neutron halo nucleus  $^{11}\text{Li}$  [11] and recently that of the four-neutron halo nucleus  $^8\text{He}$  [12] were determined based on these calculations. The results are now benchmark tests for nuclear structure theory.

*Ab initio* descriptions of the structure of light nuclei based on realistic two- and three-nucleon interactions between individual nucleons have been developed during the past years. Such are Greens-Function Monte-Carlo (GFMC), Fermionic Molecular Dynamics (FMD), and Large Basis No-Core Shell Model (NCSM) calculations, which have predicted nuclear charge radii of beryllium isotopes. Moreover, the charge radius of  $^7\text{Be}$  gives constraints for the determination of the  $^7\text{Be}(p, \gamma)^8\text{B}$   $S$ -factor that is crucial for solar neutrino experiments [13, 14]. For these reasons, the isotope shift of beryllium isotopes has recently attracted considerable interest. Measurements

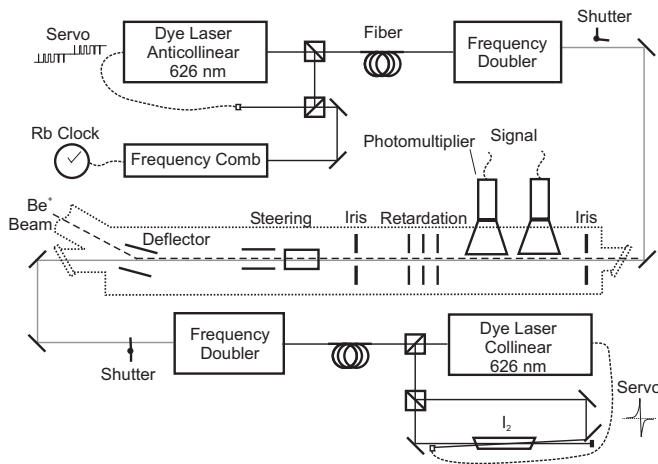


FIG. 1: Setup for collinear laser spectroscopy with parallel and antiparallel excitation and a frequency comb for reference.

on trapped and cooled ions in a Paul trap have been proposed for the D1 line [15] and first results in the D2 line were reported [16]. However, these measurements have not yet reached the accuracy required to extract the field shift.

We have developed a technique to determine the optical transition frequencies in collinear laser spectroscopy and used it for on-line measurements on  ${}^{7,9,10,11}\text{Be}$ . The radioactive isotopes were produced at ISOLDE (CERN) with a 1.4 GeV proton beam impinging on a uranium carbide target. Beryllium atoms were ionized with the laser ion source (RILIS). After extraction, acceleration to 50 kV and mass separation, the ions were delivered to the collinear laser spectroscopy setup [18]. This has been used for isotope-shift measurements on many elements down to neon ( $Z = 10$ ) [19]. However, for very light elements the systematic uncertainties caused by the measurement of the acceleration voltage exceed the nuclear volume effect. Now, we can overcome these limitations employing a frequency comb and measuring the absolute transition frequencies  $\nu_p$  for parallel and  $\nu_a$  for antiparallel geometry of ion and laser beams. This yields the rest frame frequency  $\nu_0$  independently of the acceleration voltage via the relativistic formula  $\nu_0^2 = \nu_p \cdot \nu_a$ .

A schematic layout of the setup and the laser system is shown in Fig. 1. The ion beam is superimposed with the co- and counter-propagating laser beams by an electrostatic  $10^\circ$  deflector. The laser beams enter and leave the beamline through a pair of Brewster windows. Two adjustable irises and further sets of fixed size apertures down to 5 mm diameter are used along the beam line to ensure good overlap and to avoid stray light in the optical detection region. Doppler tuning is performed by changing the potential of the detection region in the range of  $\pm 10$  kV. Two photomultipliers are used for resonance fluorescence detection.

The output of two dye lasers was frequency-doubled to

produce ultraviolet light at 313 nm and the UV beams were well collimated over a distance of about 8 m with a beam diameter of about 3-4 mm, well adapted to the ion beam size. To avoid strong optical pumping and saturation broadening of the induced transitions, the UV light was attenuated to less than 5 mW. The fundamental light at 626 nm for collinear and anti-collinear excitation was frequency-stabilized in different ways. One of the dye lasers was locked to an iodine line using frequency modulation saturation spectroscopy, while the second one was locked to a frequency comb (Menlo Systems FC1500). During the beamtime, the frequency of the iodine-locked laser was repeatedly measured with the frequency comb. In total, 12 different iodine lines were used and their frequencies measured with standard deviations on the order of 20 kHz. The Rb clock that was used as a reference oscillator for the frequency comb introduces an additional systematic uncertainty of about 350 kHz. However, this contribution cancels out for the isotope shifts in which frequency differences are evaluated.

Measurements were performed with the frequency of the collinear laser locked to a suitable iodine line. The voltage of the detection region was tuned to record the hyperfine-structure pattern of the collinear excitation. Then, the frequency of the anti-collinear dye laser was locked to the frequency comb and its frequency chosen such that the resonance pattern was covered by the same voltage range. Repetitive scanning was performed by tuning the voltage across this range. Dwell times of 20 ms per step were used, resulting in about 4 s per scan. Two remote-controlled mirrors were used to block alternately one of the two laser beams during each scan. Typically  $2 \times 50$  scans were accumulated for isotopes with high yields, whereas up to  $2 \times 400$  scans were taken for a spectrum of  ${}^{11}\text{Be}$  (see Fig. 2).

The spectra were fitted with Voigt profiles of common widths for all hyperfine structure components. The hyperfine pattern was reproduced by direct calculation of the  $F \rightarrow F'$  resonance position from

$$\nu_{FF'} = \nu_{\text{cg}} + \frac{1}{2} [A_{2p} C(F, I, J) - A_{2s} C(F', I, J)] \quad (1)$$

with the center-of-gravity frequency  $\nu_{\text{cg}}$ , the  $A$  factors of the ground ( $A_{2s}$ ) and excited states ( $A_{2p}$ ), respectively, and  $C(F, I, J) = F(F+1) - I(I+1) - J(J+1)$ . Chi-square-minimization was done by varying  $A$  and  $\nu_{\text{cg}}$  amongst other parameters. Weak satellite peaks arising at higher acceleration voltages due to inelastic collisions with residual gases were also included in the fitting function. The achievable accuracy was tested in an off-line beamtime and systematic shifts of the transition frequency evaluated. Only a small effect caused by beam misalignments could be observed.

The obtained isotope shifts  $\delta\nu_{\text{IS}}^{9,A} = \nu_0({}^A\text{Be}) - \nu_0({}^9\text{Be})$  are listed in Tab. I. The quoted uncertainty represents the standard error of the mean of individual results from

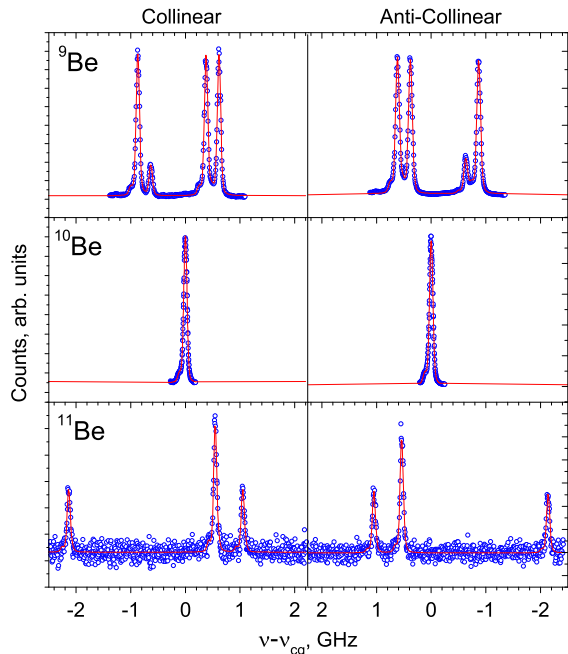


FIG. 2: (Color online) Fluorescence spectra ( $\circ$ ) for  ${}^{9,10,11}\text{Be}^+$  in the  $2s_{1/2} \rightarrow 2p_{1/2}$  transition as a function of the Doppler-tuned frequency in collinear (left) and anti-collinear (right) excitation. Frequencies are given relative to the respective hyperfine-structure center of gravity for the odd isotopes and the resonance frequency for  ${}^{10}\text{Be}$ . Lines (—) are fitting results for Voigt profiles as discussed in the text.

all measurements on a particular isotope. An uncertainty of 0.5 MHz accounting for possible misalignments of the laser and ion beam overlap was added quadratically. Recoil corrections in the isotope shift are only at the 10% level of the final uncertainty. Charge radii are deduced by subtracting the mass-dependent isotope shift of the respective isotope pair as calculated in Ref. [7]. The remaining nuclear-volume shift provides the change in the mean-square nuclear charge radius  $\delta \langle r_c^2 \rangle$  between two isotopes. Absolute charge radii  $r_c$  must be related to at least one isotope for which the absolute radius is known and can then be deduced according to

$$r_c^2({}^A\text{Be}) = r_c^2({}^9\text{Be}) + \frac{\delta\nu_{\text{IS}}^{9,A} - \delta\nu_{\text{MS}}^{9,A}}{C} \quad (2)$$

with the theoretically calculated electronic factor  $C = -16.912 \text{ MHz/fm}^2$  [7].

For stable  ${}^9\text{Be}$ ,  $r_c$  was determined by elastic electron scattering [17], and by muonic atom spectroscopy [20]. Reported charge radii of 2.519(12) fm [17] and 2.39(17) fm differ by 0.13 fm but agree within the rather large uncertainty of the muonic atom result. We have used the electron scattering result, but we note that this was not obtained in a completely nuclear-model indepen-

TABLE I: Isotope shifts  $\delta\nu_{\text{IS}}^{9,A}$  in the D1 line and theoretical mass shifts  $\delta\nu_{\text{MS}}^{9,A}$  [7, 8] for  ${}^A\text{Be} - {}^9\text{Be}$ . Uncertainties for the absolute charge radius  $r_c$  include the uncertainty in the reference radius  $r_c({}^9\text{Be}) = 2.519(12) \text{ fm}$  [17].

	$\delta\nu_{\text{IS}}^{9,A}$ , MHz	$\delta\nu_{\text{MS}}^{9,A}$ , MHz	$\delta \langle r_c^2 \rangle^{9,A}$ , fm <sup>2</sup>	$r_c$ , fm
${}^7\text{Be}$	-49 236.9(9)	-49 225.75(4)	0.66(5)	2.647(17)
${}^9\text{Be}$	0	0		2.519(12)
${}^{10}\text{Be}$	17 323.8(13)	17 310.44(1)	-0.79(8)	2.357(18)
${}^{11}\text{Be}$	31 565.0(9)	31 560.31(6)	-0.28(5)	2.463(16)

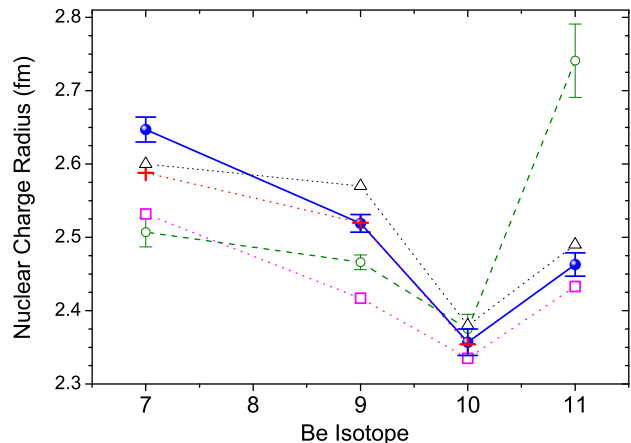


FIG. 3: (Color online) Experimental charge radii of beryllium isotopes from isotope-shift measurements ( $\bullet$ ) compared with values from interaction cross-section measurements ( $\circ$ ) and theoretical predictions: Greens-Function Monte-Carlo calculations ( $+$ ) [2, 22], Fermionic Molecular Dynamics ( $\Delta$ ) [23], *ab initio* No-Core Shell Model ( $\square$ ) [14, 24, 25].

dent way. Hence, reanalysis of the Be scattering data, as performed for the proton [21], would be useful to determine whether the small uncertainty of 0.012 fm is reliable. However, a small change in the reference radius causes primarily only a parallel shift of all charge radii.

Results for  $\delta \langle r_c^2 \rangle$  and  $r_c$  are listed in Table I. Isotope shifts in the D2 line have also been measured and are still under evaluation. The extracted charge radii agree with the values reported here, but are less accurate due to unresolved hyperfine structures.

The derived nuclear charge radii are shown in Fig. 3:  $r_c$  decreases from  ${}^7\text{Be}$  to  ${}^{10}\text{Be}$ , but then increases for  ${}^{11}\text{Be}$ . The decrease is probably caused by the clusterization of  ${}^7\text{Be}$  into an  $\alpha$ - and a triton-cluster, whereas  ${}^9,{}^{10}\text{Be}$  are considered to be  $\alpha + \alpha + n$  and  $\alpha + \alpha + n + n$  systems, respectively, and are more compact. According to a simple frozen core two-body model the increase from  ${}^{10}\text{Be}$  to  ${}^{11}\text{Be}$  can be attributed to the motion of the  ${}^{10}\text{Be}$  core relative to the center of mass. Using  $r_c^2({}^{11}\text{Be}) = R_{\text{cm}}^2 + r_c^2({}^{10}\text{Be})$  a rms distance of 7.0 fm between the neutron and the center of mass of  ${}^{11}\text{Be}$  can be extracted directly from  $\delta \langle r_c^2 \rangle$ .

TABLE II: Magnetic dipole coupling constants  $A$  of the  $2s_{1/2}$  and the  $2p_{1/2}$  states and the magnetic moments of the odd isotopes.

Isotope	$A_{2s}$ (MHz)	$A_{2p}$ (MHz)	$\mu(\mu_N)$	Ref.
${}^7\text{Be}$	-742.90(25)	-140.17(18)	-1.3995(5) -1.398(15)	this [29]
${}^9\text{Be}$	-624.97(4)	-118.00(4)		this
	-625.008837048(10)	-118.6(36)	-1.177432(3)	[30, 31]
${}^{11}\text{Be}$	-2677.4(8)	-505.4(5)	-1.6813(5) -1.6816(8)	this [32]

To test nuclear-structure theories, predictions from different models are included in Fig. 3. Reported point-proton radii  $r_{pp}$  were converted to nuclear charge radii  $r_c$  by folding in proton  $R_p$  [21] and neutron  $R_n$  [26] rms charge radii and adding the Darwin-Foldy term [27] :

$$\langle r_c^2 \rangle = \langle r_{pp}^2 \rangle + \langle R_p^2 \rangle + \frac{N}{Z} \langle R_n^2 \rangle + \frac{3\hbar^2}{4m_p^2 c^2}. \quad (3)$$

Nuclear-model dependent charge radii extracted from interaction cross-section measurements [28] show a similar trend as our data but changes are smaller for the isotopes below  ${}^{10}\text{Be}$  and overestimated for  ${}^{11}\text{Be}$ . All theoretical model predictions show good agreement with our results. Depending on the model, specific features are especially well reproduced. In the case of GFMC calculations [2, 22] the agreement for  ${}^9, {}^{10}\text{Be}$  is striking whereas the decrease between  ${}^7\text{Be}$  and  ${}^9\text{Be}$  is slightly underestimated. Unfortunately, a charge radius calculation for  ${}^{11}\text{Be}$  has not been obtained to date. FMD [23] and improved NCSM [14, 24, 25] calculations include the halo nucleus and the change between  ${}^{10}\text{Be}$  and  ${}^{11}\text{Be}$  is very well predicted. Concerning the other isotopes FMD does a better job for the isotope pair  ${}^9, {}^{10}\text{Be}$ , whereas the change in the pair  ${}^7, {}^9\text{Be}$  is best described by the NCSM results (note that the absolute charge radius depends on the reference radius).

From fitting the observed hyperfine structures we obtain the magnetic dipole constant  $A$  for the  $2s$  and the  $2p_{1/2}$  states as listed in Tab. II. Based on the precision measurement of  $A_{2s}$  in  ${}^9\text{Be}$  [30] and the corresponding nuclear magnetic moment  $\mu = -1.177432(3)\mu_N$  [31], we determine the magnetic moments of  ${}^7\text{Be}$  and  ${}^{11}\text{Be}$ . For  ${}^{11}\text{Be}$  we confirm the previously measured value from an optical pumping  $\beta$ -NMR experiment [32]. For  ${}^7\text{Be}$ , an earlier value from optical hyperfine measurements [29] is improved by more than an order of magnitude.

To summarize, we have measured the charge radii of  ${}^7, {}^9, {}^{10}, {}^{11}\text{Be}$  with on-line frequency-comb based collinear laser spectroscopy. From a simple frozen-core two-body model we obtain a rms distance of about 7 fm between the halo neutron and the center of mass in  ${}^{11}\text{Be}$ . Comparison with elaborate nuclear structure calculations (GFMC, FMD, and LBSM) shows in all cases good agreement

with our measurement. The magnetic moment of  ${}^{11}\text{Be}$  has been confirmed and the accuracy for  ${}^7\text{Be}$  considerably improved. The developed experimental technique has the potential to be applied to the very short-lived nuclei  ${}^{12}, {}^{14}\text{Be}$  and can generally improve the accuracy of collinear laser spectroscopy where this is required.

This work was supported by the Helmholtz Association (VH-NG-148), BMBF (06TU263I, 06MZ215, 06UL264I), and the EU (FP-6 EU RII3-CT-2004-506065). M.K. was supported by the EU (MEIF-CT-2006-042114). We gratefully acknowledge technical support by M. Fischer and R. Holzwarth from Menlo Systems and by the ISOLDE technical group.

- 
- [1] I. Tanihata *et al.*, Phys. Rev. Lett. **55**, 2676 (1985).
  - [2] S. C. Pieper and R. B. Wiringa, Ann. Rev. Nucl. Part. Sci. **51**, 53 (2001).
  - [3] R. Neugart *et al.*, Phys. Rev. Lett. **101**, 132502 (2008).
  - [4] Z.-C. Yan and G. W. F. Drake, Phys. Rev. A **61**, 022504 (2000).
  - [5] Z.-C. Yan and G. W. F. Drake, Phys. Rev. Lett. **91**, 113004 (2003).
  - [6] M. Puchalski, A. M. Moro, and K. Pachucki, Phys. Rev. Lett. **97**, 133001 (2006).
  - [7] Z. C. Yan, W. Nörtershäuser, and G. W. F. Drake, Phys. Rev. Lett. **100**, 243002 (2008).
  - [8] M. Puchalski and K. Pachucki, Phys. Rev. A **78**, 052511 (2008).
  - [9] G. Ewald *et al.*, Phys. Rev. Lett. **93**, 113002 (2004).
  - [10] L.-B. Wang *et al.*, Phys. Rev. Lett. **93**, 142501 (2004).
  - [11] R. Sánchez *et al.*, Phys. Rev. Lett. **96**, 033002 (2006).
  - [12] P. Mueller *et al.*, Phys. Rev. Lett. **99**, 252501 (2007).
  - [13] A. Csoto and K. Langanke, Nucl. Phys. A **636**, 240 (1998).
  - [14] P. Navrátil, C. A. Bertulani, and E. Caurier, Phys. Rev. C **73**, 065801 (2006).
  - [15] M. Záková *et al.*, Hyperf. Interact. **171**, 189 (2006).
  - [16] T. Nakamura *et al.*, Phys. Rev. A **74**, 052503 (2006).
  - [17] J. A. Jansen, R. Th. Peerdeman and C. de Vries, Nucl. Phys. A **188**, 337 (1972).
  - [18] R. Neugart, Nucl. Instr. Meth. **186**, 165 (1981).
  - [19] W. Geithner *et al.*, Hyperf. Interact., **129**, 271 (2000).
  - [20] L. A. Schaller *et al.*, Nucl. Phys. A **343**, 333 (1980).
  - [21] I. Sick, Phys. Rev. Lett. B **576**, 62 (2003).
  - [22] S.C. Pieper, K. Varga and R.B. Wiringa, Phys. Rev. C **66**, 044310 (2002).
  - [23] R. Torabi, GSI, priv. comm. (2008).
  - [24] C. Forssén, P. Navrátil, W.E. Ormand, and E. Caurier, Phys. Rev. C **71**, 044312 (2005).
  - [25] P. Navrátil, priv. comm. (2008).
  - [26] S. Kopecky *et al.*, Phys. Rev. C **56**, 2229 (1997).
  - [27] J. L. Friar, J. Martorell, and D. W. L. Sprung, Phys. Rev. A **56**, 4579 (1997).
  - [28] I. Tanihata *et al.*, Phys. Lett B **206**, 592 (1988).
  - [29] S. Kappertz *et al.* in ENAM98: Exotic Nuclei and Atomic Masses, B. M. Sherrill *et al.* (Eds.), AIP 110 (1999).
  - [30] D. J. Wineland, J. J. Bollinger, and W. M. Itano, Phys. Rev. Lett. **50**, 628 (1983).
  - [31] W. M. Itano, Phys. Rev. B **27**, 1906 (1983).

[32] W. Geithner *et al.*, Phys. Rev. Lett. **83**, 3792 (1999).